# Design of the Electric Powertrain System of a Fully Autonomous Small Vessel

Pedro Afonso Fragoso Coelho Henriques de Carvalho
pedro.h.carvalho@tecnico.ulisboa.pt

Instituto Superior Técnico, Lisboa, Portugal

June 2022

**Abstract**

This work follows the development of an unmanned surface vehicle (USV), focusing on the present propulsion system, developed by Escola Superior Náutica Infante D. Henrique. The system to be modeled is comprised of two sets of DC motor and propeller, and a hull. The DC motor is characterized using its equivalent electric circuit, whose parameters are experimentally obtained. By designing experimental tests that isolate each parameter it is possible to estimate and validate, through the construction of a preliminary model using steady state and transient state validation. After defining the behaviour of the USV's dynamics, *i.e.*, equilibrium of forces, with one degree of freedom, it is possible to characterize the propellers through theoretical analysis and experimental testing and the hull through theoretical analysis. For the propellers experimental characterization, one experimental setup was developed and tested in a water channel. The model is then calibrated and added a simplified model of the batteries. Based on the developed models, a preliminary assessment is carried to the USV capabilities and limitation.
**Keywords:** Unmanned surface vehicle, Electric propulsion, Parameter estimation, DC motors, Propellers

## 1. Introduction

In the second half of the 20th century, the concern about sustainability of fossil fuels become a hot topic [12]. This concern still persists as the fossil fuel consumption as been almost consistently increasing to this day [11]. The transport sector is responsible to a large sum of greenhouse gases emissions. Battery powered electric vehicles have shown to be a more environmental friendly option. More even when the electricity used to power said batteries originates from a clean source, like solar and wind [7].

The technological advances of nautical transportation systems propelled the creation of a new type of vessel to operate on water's surface, that does not need direct human intervention, *i.e.*, unmanned surface vehicles (USV). As the name suggests, a USV is a vessel, usually of reduced dimensions, that operates on the surface of the water without a crew onboard [14]. The ability to perform intensive and repetitive activities, that are not encouraging for humans, in an autonomous way is appreciated. On the other hand the user is also distanced from danger and risky campaigns.

To obtain a more sustainable transportation system, the electrification of the nautical transportation is align with the *2030 Agenda for Sustainable Development* towards the mitigation of the climate change. This 2030 Agenda for Sustainable Development is a document signed by United Nations in 2015 by 195 nations to improve people's lives [10].

*Escola Superior Náutica Infante D. Henrique* (ENIDH) in partnership with *Instituto Superior Técnico*, amongst other entities, is developing a fully electric USV. The project aims to encourage and contribute to technological advances and relevant work in the various fields involved in the making of such vessel. It also establishes a platform where students can have the opportunity to learn important matters and enlarge their skill set.

## 2. Background

Although the idea of USVs can be attributed to the WWII, used for military purposes, one of the pioneers was the Massachusetts Institute of Technology (MIT). In 1993 they developed their first craft, the *ASC ARTEMIS*, part of MIT's Sea Grant Program . It was a 1/17 scale replica of a fishing trawler intended to provide a study platform for command and control architectures, navigation systems and basic data collection techniques [8]. The second project from MIT, the *ASC ACES*, was a fully new design, a more capable one. The *ASC ACES* was later renamed *Autocat* when the gaso-

line engines were discarded and the propulsion was upgraded to electric motors [13].

*Sesamo* is of special interest [3], because of its success as a catamaran style hull and fully electric USV. Destined to study the sea-air interface on the Terra Nova Bay area in an Italian expedition to Antarctica in 2004, part of the Italian National Program of Research in Antarctica (PNRA), by monitoring air and water samples. This small vessel comprised of a catamaran hull, instrumentation and electric power train using 4 lead batteries, a DC/DC converter and two electrical thrusters allowing maneuverability by employing differential propeller revolution rates.

*Artemis* although serving well as a testing platform and successfully demonstrating the ability to operate autonomously and collect hydrographic data, *Artemis*' performance was severely affected by its reduced dimensions. Limited endurance and seakeeping ability were the main consequences [9], which made it unsuitable for coastal and open ocean research [8]. The newer iteration, *ACES* and later *AutoCat*, had as goal to solve the problems observed in *Artemis*, using a greater size catamaran-hull to provide better roll stability and greater payload capacity [13]. This new model successfully completed a survey in the Boston Harbor in December, 1997 [9].

During sea trials in the Genoa harbour and in Terra Nova Bay, *Sesamo* showed its ability to operate autonomously, following a set of way points, set manually by a human operator, and successfully performing onboard water sampling [2].

Since 2018, the *Centro de Investigação e Desenvolvimento* (CID) of ENIDH, is developing a project named *USV-enautica1*. This vessel is the flag-ship of one of ENIDH's more recent projects, sea2future, that aims at promoting research in applied maritime robotics. The *USV-enautica1*, shown in Figure 1., is the first iteration of an USV developed by ENIDH, which is mainly developed by students and professors, to acquire expertise in various fields.

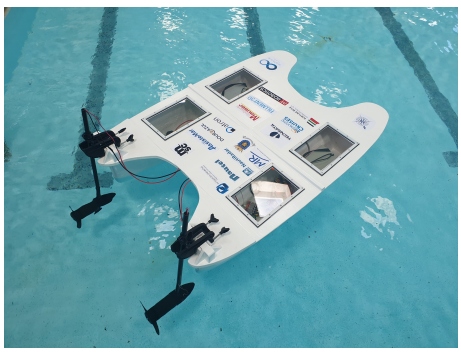

Figure 1: ENIDH's USV-enautica1.

## 3. USV Propulsion system

The *USV-enautica1* system consists of a hull, powertrain and electronics, the latter mainly for navigation and measurements purpose. Only the hull and powertrain are in the scope of this work. The catamaran-style hull houses the batteries and electronics in its hollow interior and supports the motors on its rear. The hull's dimensions are shown in Table 1.

| Dimensions | |
|---|---|
| Length | 215.5cm |
| Beam | 137.2cm |
| Height | 45.0cm |
| Draft | 24.9cm |
| Wetted surface | 9485.6cm$^2$ |

Table 1: *USV-enautica1*'s dimensions.

The powertrain is comprised of two lead-acid batteries, to supply the power needed by the electric motors, a DC/DC converter to control the electric motors and two sets of DC motor and a propeller, to provide thrust and differential maneuverability. Figure 2. shows the block diagram of the power train.

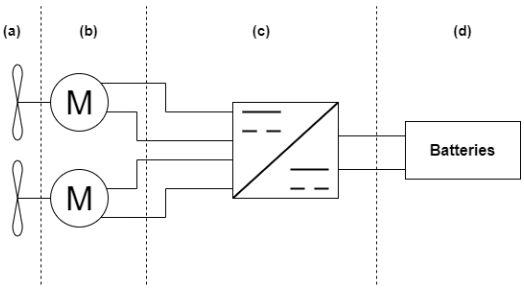


Figure 2: Powertrain block diagram, (a)-Propellers, (b)-DC motors, (c)-DC/DC converter, (d)-Batteries.

The two DC motors convert the electric power provided by the batteries into mechanical power for the propellers. In this project the motors used are Permanent Magnet DC (PMDC) motors. Table 2 shows the DC motor specifications.

| DC motor | | Propeller | |
|---|---|---|---|
| Rated voltage | 12V | Maximum thrust | 245N |
| Rated current | 50A | Diameter | 28cm |
| | | Number of blades | 2 |

Table 2: DC motor and Propeller specifications provided by the manufacturer

The propellers take the torque generated by the DC motor and convert it in usable force that acts on the water and propels the vessel. Table 2 shows the propeller specifications and Table 3 shows the mass of each system's component.

| Component | Mass [kg] |
|---|---|
| Hull | 30 |
| Motor + Propeller | 4 x 2 |
| Electronics | 1 |
| Battery | 30 x 2 |
| Total | 99 |

Table 3: Mass of each component

The main target of this work is to develop a preliminary model of the USV dynamics, focusing on the hull and the electric motor coupled to the propellers, as shown in Figure 3. In this model, the input is the desired linear velocity of the vessel, $v$. From it, the required propeller thrust, $F$, mechanical torque, $T$, and rotational speed, $\omega_r$, are estimated and provided to the DC motor. Knowing the required torque and speed of the DC motor, its required armature voltage, $U_a$, and current, $I_a$, are computed. Both motors will behave the same way in a 1-Dimensional space, therefore the motor simulation is done only for half of the generated force, $F$.

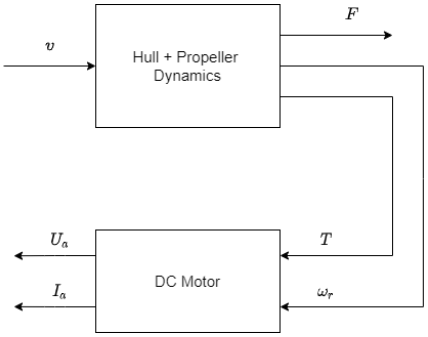


Figure 3: Model diagram.

## 4. System Modelling

### 4.1. DC Machine

#### 4.1.1 Electromechanical model

The DC motor is here represented by its equivalent circuit, according to [4]. This model was used with a parallel resistor to account for iron losses. Figure 4. and equations (1) through (8) represent the DC model behavior.

Equations (1) and (2) are obtained from the Kirchhoff laws of the DC motor equivalent circuit. In these, $I_a$ and $U_a$ are the armature current and voltage, $R_a$ and $L_a$ are the armature resistance and inductance, $\varepsilon_a$ is the electromotive force, $I'_a$ is an equivalent current representing the electromagnetic torque and $I_{fe}$ is an equivalent current representing the iron losses.

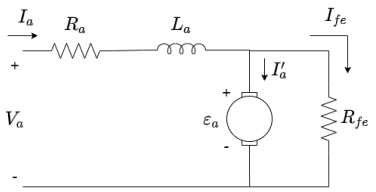


Figure 4: DC motor equivalent circuit

$$U_a = I_a R_a + L_a \frac{\mathrm{d}i_a}{\mathrm{d}t} + \varepsilon_a \tag{1}$$

$$I_a^{'} = I_a - I_{fe} \tag{2}$$

The relation between the electromotive force and the DC motor speed is given by (3), where $\omega_r$ is the angular speed of the motor and $k_\phi$ is the motor speed and torque constant.

$$\varepsilon_a = k_\phi \cdot \omega_r \tag{3}$$

The iron losses are represented by the $R_{fe}$ resistance in the electric circuit. These can be mainly due to hysteresis and eddy current, equation (4). For simplification, and due to the typically low range of speeds used on this application, it was considered the hysteresis the main source of losses. Therefore, the iron losses can be computed using equation (5).

$$P_{fe} = k_h B^2 f = k'_h \omega_r \tag{4}$$

$$P_{fe} = U_{fe} I_{fe} = \frac{U_{fe}^2}{R_{fe}} = \frac{\varepsilon_a^2}{R_{fe}} = k'_h \cdot \omega_r \tag{5}$$

The electromagnetic torque produced by the DC motor, $T_e$ in equation (6) and (7), will be converted into angular acceleration, mechanical losses, $P_{mec}$, and useful load torque, $T_l$, which will be provided to the propeller.

$$T_e = J \frac{\mathrm{d}\omega_r}{\mathrm{d}t} + \frac{P_{mec}}{\omega_r} + T_L \tag{6}$$

$$k_\phi I_a - k'_h = J \frac{\mathrm{d}\omega_r}{\mathrm{d}t} + \beta \omega_r + T_L \tag{7}$$

Note that $k'_h = 0 \quad \text{if} \quad \omega_r = 0$.

Finally, the power balance equation is given by (8), where $P_{in}$ is the input DC power, $P_{cu}$ is the copper losses, represented by the voltage drop in armature resistance and $P_{out}$ the useful power generated and delivered to the propeller.

$$P_{in} = P_{cu} + P_{fe} + P_{mec} + P_{out} \tag{8}$$

#### 4.1.2 Estimation of unknown variables

In order to produce the model a series of experimental tests were performed to estimate each set of unknown variables.

To perform the tests needed, the DC motor was supplied by a DC power supply coupled with a switch., for "start up's" and "cut off's".

Note that all tests in this section were executed without external load, *i.e.*, $T_L = 0$ and subsequently $P_{out} = 0$.

**Armature Resistance, $R_a$**

It was used an indirect method based on the equivalent circuits' equations

This test was ran in steady state and with the maximum voltage possible before the motor started moving, *i.e.*, $\varepsilon_a = 0$ and $L\frac{\mathrm{d}i_a}{\mathrm{d}t} = 0$. With the values of the armature current and voltage, the armature resistance can be computed, equation (9).

$$U_a = I_a R_a \tag{9}$$

The armature resistance was computed for different positions of the rotor. The average value of 0.176Ω was then used for the model.

**Motor speed and torque constant, $k_\phi$**

Similarly to the calculation of the armature resistance, the same indirect method was utilized, the only difference being that the rotor was allowed to move freely, which means that equation (1) can be used.

And by rearranging equation (1), the value of the constant can be computed, using equation (10).

$$k_\phi = \frac{U_a - I_a R_a}{\omega_r}, \omega_r = \frac{2\pi N_r}{60} \tag{10}$$

Using different speeds, this constant was determined. The average value of 0.0907Wb was used for the simulation of the system.

**Hysteresis coefficient, $k'_h$, and mechanical losses coefficient, $\beta$**

It is possible to estimate $k'_h$ and $\beta$ by observing the relation between input power and speed. At no load, equation (8) is reduced to:

$$P_{in} = P_{cu} + P_{fe} + P_{mec} \tag{11}$$

By subtracting the copper losses from (11), the remain power will have a linear and a quadratic behavior with the speed, shown in equations (12) and (13). The results for the Iron and mechanical losses are shown in figure (5).

$$P_{fe} = k'_h \omega_r \tag{12}$$

$$P_{mec} = \beta \omega_r^2 \tag{13}$$

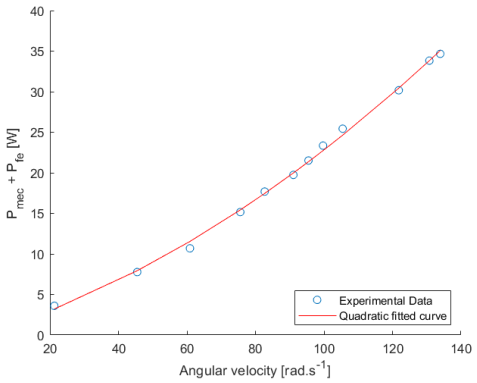


Figure 5: DC motor's mechanical and iron losses.

A quadratic fitting was applied resulting in an expression of the form $ax + bx^2$ that complies with the expression $k'_h\omega_r + \beta\omega_r^2$ $a = k'_h = 0.1293$W·s and $b = \beta = 9.895\text{x}10^{-4}$N·m·s.

**Armature Inductance, $L_a$**

For the calculation of the armature inductance, $L_a$, the rotor was stopped and a voltage step was applied to the DC motor. This will lead to a transient current. At the start-up moment, with the rotor stopped, equation (1) results in (14).

$$U_a = I_a R_a + L_a \frac{\mathrm{d}i_a}{\mathrm{d}t} \tag{14}$$

The current during the machine start up was recorded and represented in orange is the linear section chosen, as shown in Figure 6. For the calculation it is needed the peak voltage ($U_a = 13.6$ V), peak current ($I_a = 5.68$ A) and the derivative taken from the orange section ($\frac{\mathrm{d}i_a}{\mathrm{d}t} = 14055$ A/s), substituting on (14) results in $L_a = 8.965\text{x}10^{-4}$ H.

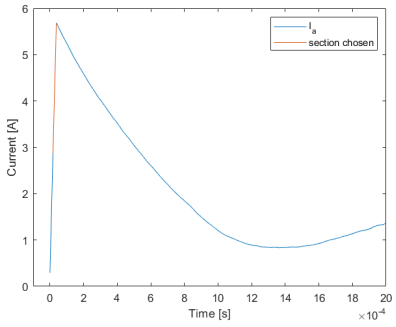


Figure 6: DC motor's transient(during start up) armature current.

**Coefficient of inertia, $J$**

The coefficient of inertia, $J$, was estimated from the stopping transient of the DC motor. With the motor running, the power supply is disconnected, Without current, no electromagnetic torque is applied, and equation (7) becomes (15).

$$J\frac{\mathrm{d}\omega_r(t)}{\mathrm{d}t} + \beta\omega_r(t) + k'_h = 0 \tag{15}$$

That can be solved by following equation (16) form:

$$\omega_r(t) = \omega_{rf}(t) + \omega_{rn}(t) \tag{16}$$

Where, $\omega_{r_f}$ is the forced solution and $\omega_{r_n}$ is the natural solution. $A$ is a constant.

$$\omega_{rf} = -\frac{k_h}{\beta} \tag{17}$$

$$\omega_{rn}(t) = Ae^{-\frac{\beta}{J}t} \tag{18}$$

The absence of current gives the relation of voltage and speed as described in equation (1), so it was possible to obtain the evolution of the speed from the evolution of the armature voltage, as shown in Figure 7. The relation presented only begins after the voltage drop, due to the armature resistance, that happens roughly at 0s when the power supply is turned off. The orange section shows the linear portion used in the study of the variable of interest. For it, the section was considered linear and $t = 0$ the beginning of that section. This results in $A = 320.54$ and $J = 7.235\text{x}10^{-4}$ kg·m$^2$.

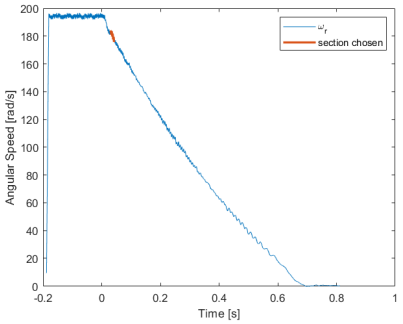


Figure 7: DC motor's angular speed during supply cut off transient.

### 4.1.3 Validation

To test and validate the DC motor model, a preliminary model was developed in SIMULINK environment, where $U_a$ and $T_L$ where chosen as inputs and $I_a$ and $\omega_r$ as outputs, following the equations (19) and (20) and shown on the diagram in Figure 8.

$$i_a = \frac{1}{L_a}\int U_a - i_a R_a - k_\phi\omega_r\, dt \tag{19}$$

$$\omega_r = \frac{1}{J}\int k_\phi i_a - T_l - \beta\omega_r - k_h\, dt \tag{20}$$

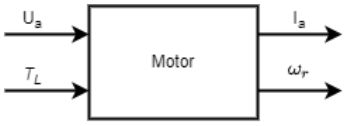


Figure 8: Preliminary model for validation of the DC motor parameters estimated.

Two types of tests were performed, one in steady state and one using a voltage step to assess the transient response. During this process the parameters estimated were tuned. Two sets of tuned values will be presented, one for each type of test.

For the steady state validation 15 experimental samples, each one corresponding to different voltage values, were set as reference and used in the simulation model. The results of the current and speed values were compared with the experimental results. The results are shown on Table 4. The steady state test gives satisfactory results, as it was obtained a low percentage mean relative error for the current and besides a higher error for the motor speed, not only it is mostly notable in lower speeds as it may also be justified by the low accuracy of the measuring process.

| $U_a$ (V) | $I_a(exp)$ (A) | $I_a(est)$ (A) | $\lvert\%error_{I_a}\rvert$ | $N_r(exp)$ (rpm) | $N_r(est)$ (rpm) | $\lvert\%error_{N_r}\rvert$ |
|---|---|---|---|---|---|---|
| 2.48 | 2.06 | 2.24 | 8.60 | 91.0 | 219.7 | 141.37 |
| 3.80 | 2.30 | 2.39 | 4.03 | 203.3 | 355.7 | 75.03 |
| 5.30 | 2.46 | 2.57 | 4.45 | 434.3 | 510.4 | 17.51 |
| 6.27 | 2.56 | 2.68 | 4.84 | 581.3 | 610.4 | 5.00 |
| 7.55 | 2.74 | 2.83 | 3.42 | 721.7 | 742.4 | 2.87 |
| 8.21 | 2.84 | 2.91 | 2.52 | 789.7 | 810.4 | 2.63 |
| 8.77 | 2.9 | 2.98 | 2.69 | 869.7 | 868.2 | 0.17 |
| 9.15 | 2.99 | 3.02 | 1.09 | 911.7 | 907.3 | 0.47 |
| 9.63 | 3.03 | 3.08 | 1.62 | 952.3 | 956.8 | 0.47 |
| 10.11 | 3.10 | 3.14 | 1.11 | 1007.0 | 1006.3 | 0.07 |
| 11.12 | 3.26 | 3.25 | 0.18 | 1163.3 | 1110.4 | 4.55 |
| 11.85 | 3.38 | 3.34 | 1.18 | 1248.7 | 1185.7 | 5.04 |
| 12.13 | 3.37 | 3.37 | 0.09 | 1279.0 | 1214.6 | 5.03 |
| | mean | | 2.56 | mean | | 18.59 |

Table 4: Steady state validation results

Table 5. shows the tuned values relative to the the steady state validation. The X represents that no tuning was necessary for the specified parameter.

| $R_a$ [Ω] | $k_\phi$ [Wb] | $k_h$ [W·s] | $\beta$ [N·m·s] | $L_a$ [H] | $J$ [kg·m$^2$] |
|---|---|---|---|---|---|
| X | X | 0.1802 | $9.895\text{x}10^{-4}$ | X | X |

Table 5: DC motor tuned parameters result of steady state validation.

The transient state validation consisted on the evaluation and comparison of the transient behavior of the DC motor, when a voltage step is applied.

The motor was experimentally submitted to a 9.5V voltage step. To test the model, the experimental voltage was used as the model input and since there is no external load it is known that $T_L = 0$. Subsequently both currents are compared, the experimental one and the simulated one.

In Figure 9.(a) and 9.(b) it is shown both experimental and simulated voltage and current, respectively, in Figure 10.(a) the simulated velocity and in Figure 10.(b) the relative error of both current curves in time. To reduce the noise produced by the model, the voltage curve used in the simulation was smoothed using a moving average filter. Although the error seen in Figure 10.(b) during the transient period is considerably high, by inspecting Figure 9.(b), the error can be considered low in a pratical point of view as the simulated current reaches virtually the same peak value, having only a higher time constant. Then when it reaches steady state the error decreases to an average value of 4.13%, this value for the entire curve is 11.59% which can be also considered satisfactory. The speed value seen in Figure 10,(a) although being higher than the steady state value found for a similar voltage in Table 4., it may occur due to differences in motor temperatures due to long periods of testing.

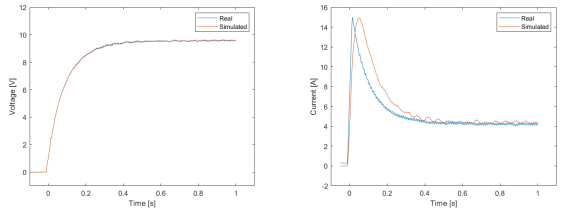


(a) Voltage (b) Current

Figure 9: DC motor's real and simulated transient during transient state validation.

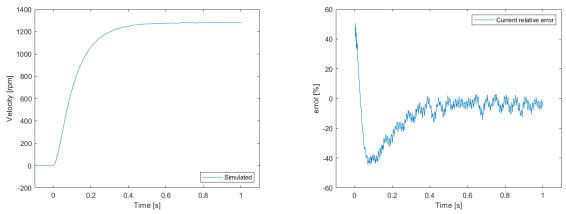


(a) Speed (b) Relative error

Figure 10: DC motor's speed and relative error during transient state validation.

Table 6. shows the tuned values relative to the the transient state validation. The X represents that no tuning was necessary for the specified parameter.

| $R_a$ ($\Omega$) | $k_\phi$ (Wb) | $k_h$ (W·s) | $\beta$ (N·m·s) | $L_a$ (H) | $J$ (kg·m$^2$) |
|---|---|---|---|---|---|
| X | 0.0656 | 0.1810 | 7.875x10$^{-4}$ | 8.964x10$^{-4}$ | 8.682x10$^{-4}$ |

Table 6: DC motor tuned parameters result of transient state validation.

From this point onwards the values used for the estimated parameters are the ones corresponding to Table 5. The values in Table 5 are preferred since the upcoming simulations were done in steady state.

## 4.2. Hydrodynamic system

### 4.2.1 Model

Regarding the scope of this project, a model with only 1 degree of freedom was considered to represent the vessel dynamics.

The equilibrium of forces is given by equation (21) according to [5] and illustrated in Figure 11. Where $R$ is the drag force ($R = \frac{1}{2}\rho_w A_w C_T v^2$), $F$ is the thrust and $v$ is the USV linear speed. In (21) $m$ is the USV weight, $\rho_w$ is the water density, $A_w$ is the wetted surface of the USV and $C_T$ is the drag coefficient of the USV.

$$F = m\frac{\mathrm{d}v}{\mathrm{d}t} + \frac{1}{2}\rho_w A_w C_T v^2 \tag{21}$$

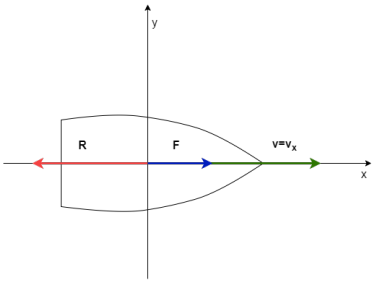


Figure 11: Illustration of the USV's equilibrium of forces.

The relation between thrust coefficient and thrust, and torque coefficient and torque are given by equations (22) and (23), respectively, according to [1]. Equation (24) defines the advance ratio, which is given by a ratio between the advance speed, $V_a$, and the propeller rotational speed, $n_r$, and the diameter, $D$. The propellers were considered with enough depth relative to the bottom of the hull so that it can be assumed $V_a$=$v_x$=$v$.

$$F = \rho_w n_r^2 D^4 K_T(J_a), \quad n_r = \frac{N_r}{60} \tag{22}$$

$$T = \rho_w n_r^2 D^5 K_Q(J_a) \tag{23}$$

$$J_a = \frac{V_a}{n_r D} \tag{24}$$

As stated in Chapter 3, the model chosen is as shown in figure 12. To obtain this, first the thrust, $F$, is calculated from equation (21). Then using equations (22) and (24) the propeller speed, $n_r$, is obtained and its torque, $T$, can be computed using (23).

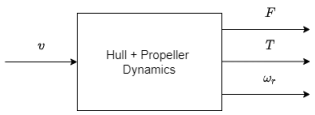


Figure 12: Hydrodynamic Model

### 4.3. Estimation of Thrust, Torque and Drag Coefficients

Similarly to section 4.1.2, the parameters of the propeller (thrust and torque coefficients) and hull (drag coefficient) are required to be estimated.

#### Thrust and Torque coefficents

An experimental methodology was used to estimate the thrust and torque propeller coefficients. The experimental setup developed is composed by two parts: a hydrodynamic and a electric feeding circuit for the electric motor. The first of the two is composed by a water channel, the propeller-motor system, a structure to hold the motor in place and a force sensor, to determine the force applied by the propeller to the water. Figure 13. shows the hydrodynamic setup schematics, the force applied, $F$, creates an opposite force in the propeller, that in turn impels the vertical shaft to rotate around the rotation point and push the sensor.

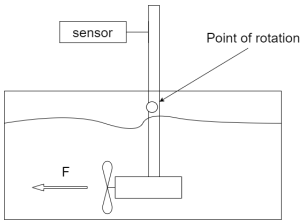


Figure 13: Hydrodynamic setup diagram.

The main electric circuit is composed by a three-phase socked connected to an autotransformer to regulate the DC motor voltage, a 3-phase step-down transformer to decrease the level of voltage to those close to the DC motor level, a full wave rectifier to convert the AC to DC voltage and a DC power supply was used to feed the force sensor. For measurement, 2 voltmeters and ammeters were used to measure the motor and voltages and an oscilloscope to measure the force sensor output.

Figure 14. shows the electric supply schematics of the DC motor.


Figure 14: Electric feeding circuit schematics.

The aim of this setup is to measure the force produced by the propellers at different rotational speeds, high current and with the propeller submerged.

To determine the thrust and torque coefficient curves it is needed to know the values of $K_T(J_a)$ and $K_Q(J_a)$ through equation (22) and (23),respectively. Regarding the advance ratio, $J_a$, for 2 blade propellers it can be approximated by a linear relation [1]. Therefore, with two points this linear regression can be estimated. Throughout the experimental period it was discovered that there was a linear relation between force and torque produced, so there was no need to calculate $K_Q$. The results presented in Table 7. are partially experimentally acquired ($U_a$,$I_a$ and $F$), partially simulated ($N_r$ and $T$) or simply calculated ($K_T$). The torque and speed were determined by using the DC model described in section 4.1 since the voltage and current were known. To account for losses between the rotor shaft and propeller it was considered a 2% torque loss.

Because the propeller is not moving relative to the water, which is to say that there is no flow and $v = 0$, from equation(24) $J_a = 0$. In order to have the first point of $K_T(J_a)$ curve, using the values of $F$ and $N_r$ from Table 7. and equation (22), the value for $K_T(J_a = 0)$ was calculated for all rows and then averaged.

| Experimental | | | Simulated | | |
|---|---|---|---|---|---|
| $U_a$[V] | $I_a$[A] | $F$[N] | $T$[Nm] | $N_r$[rpm] | $K_T(J_a = 0)$ |
| 2.32 | 4.1 | 9.64 | 0.18 | 167.1 | 0.202 |
| 3.6 | 7 | 21.59 | 0.42 | 249.1 | 0.204 |
| 4.38 | 9.26 | 28.48 | 0.62 | 289.5 | 0.199 |
| 5.09 | 11.6 | 36.55 | 0.83 | 318.7 | 0.211 |
| 5.81 | 14 | 45.69 | 1.03 | 352.4 | 0.216 |
| 6.64 | 17 | 58.88 | 1.30 | 382.5 | 0.236 |
| 7.53 | 20.3 | 72.06 | 1.58 | 418.2 | 0.242 |
| 7.75 | 20.9 | 71.52 | 1.65 | 426.9 | 0.231 |
| 7.98 | 22.2 | 77.98 | 1.74 | 430.6 | 0.247 |
| 8.71 | 24.9 | 91.43 | 2.01 | 451.8 | 0.263 |
| 9.84 | 29.6 | 110.8 | 2.43 | 482.3 | 0.279 |
| 9.86 | 30.83 | 118.33 | 2.52 | 466.4 | 0.320 |
| 10.15 | 30.45 | 115.64 | 2.49 | 502.3 | 0.269 |
| 11.09 | 35.99 | 140.39 | 2.96 | 503.2 | 0.326 |
| 12.08 | 39.98 | 153.31 | 3.33 | 529.2 | 0.322 |
| | | | | Mean | 0.250 |

Table 7: Results of the in water experiment to determine $K_T(J_a)$

The discrepancy of the various $K_T(J_a = 0)$ seen in Table 7 may exist due to high levels of perturbations felt by the propeller in the water channel that in turn affect the force sensor. This is also supported by the non linearity between $n_r^2$ and $F$ seen in Figure 15. as it contradicts the requirement set by equation (22) for the value of $K_T(J_a = 0)$ to remain the same.

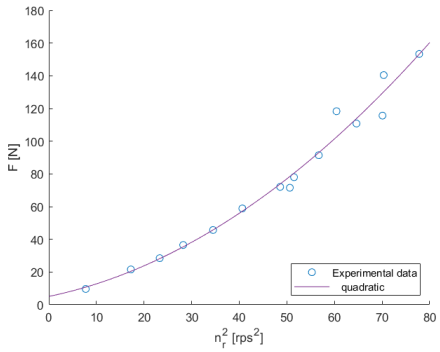


Figure 15: $F$ and $n_r^2$ relation.

The second point was obtained from experimental data gathered prior to this work, shown on table(8).

| $U_a$[V] | $I_a$[A] | $F$[N] | $T$[Nm] | $N_r$[rpm] | $v$[m/s] |
|---|---|---|---|---|---|
| 12 | 25 | 90.2 | 1.96 | 801 | 1.54 |

Table 8: Results of a prior in-water experiment.

Whilst the propeller torque and speed were simulated, the force was estimated based on the existent linearity shown in Table 7. and Figure 16. This relation is going to be used as the method to calculate the propeller generated torque, expressed in equation (25). With the values given in Table 8. it is possible to find the second point for $K_T(J_a)$ in $J_a = 0.412$, hence $K_T(J_a = 0.412) = 0.0826$. The final $K_T(J_a)$ curve is displayed in Figure 17. and equation(26).

$$T(F) = 0.0215 \cdot F + 0.0213 \tag{25}$$

$$K_T(J_a) = -0.406 \cdot J_a + 0.250 \tag{26}$$

**Drag coefficient**

Although, the total drag coefficient comprises of various parameters as of [6], to simplify, only the frictional resistive coefficient was considered for this work, as presented in equation (27), where $R_e$ is the

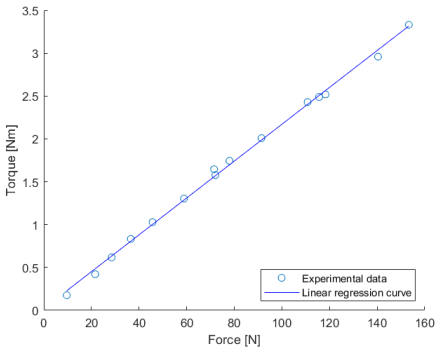


Figure 16: Force/torque relation.

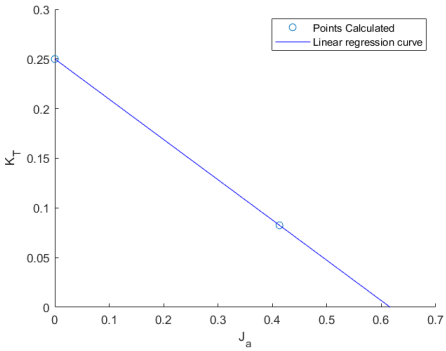


Figure 17: $K_T(J_a)$ curve

Reynolds number, $v_x$ the linear velocity, $l$ the waterline length of the ship hull and $v_w$ the kinematic viscosity of water.

$$C_T = \frac{0.075}{(log_{10}(Re) - 2)^2}, Re = \frac{v_x \cdot l}{v_w} \tag{27}$$

## 5. Discussion of the preliminary performance

### 5.1. Preliminary model and Calibration

With the DC motor and hydrodynamic systems characterized it is now possible to construct the model proposed. However, because approximations were made during the characterization stage, the model was calibrated with the experimental values from Table 8., as reference. To further complement the model, it was also calculated the input power, $P_{in}$, the output power, $P_{out}$ and the power efficiency, $\eta$, shown in equations (28) through (30), respectively, where $n$ is the number of DC motors.

$$P_{in} = U_a I_a \cdot n \tag{28}$$

$$P_{out} = T_L \omega_r \cdot n \tag{29}$$

$$\eta = \frac{P_{out}}{P_{in}} \tag{30}$$

To estimate the endurance and distance that can be travelled at a specific speed, it was considered the

total capacity of the batteries in use, $200Ah$, and a 20% efficiency loss regarding the batteries and the DC/DC converter. The system endurance and distance travelled was computed using equations (31) and (32), respectively.

$$\Delta t = \frac{Bat_{capacity}}{I_a \cdot n} \quad [h] \tag{31}$$

$$\Delta x = \Delta t \cdot v \cdot \frac{1}{1000} \quad [km] \tag{32}$$

### 5.2. Results

The simulation was run for 100 different inputs. Each input corresponds to a percentage of the linear velocity set as reference ,$v_{ref} = 1.54$ m/s (3 knots), which is the available experimental data, also corresponds to the maximum velocity that was possible to achieve. The percentage ranges from 5% to 100 % of the reference value. Table 9 shows the result of 9 simulation, Figure 18. the efficiency as function of input power for the 100 simulations, Figure 19. and 20. shows the endurance and distance travelled as a function of the percentage of reference velocity, respectively.

| % of reference | Input | Output | | | | | | | | | |
|---|---|---|---|---|---|---|---|---|---|---|---|
| | $v$(m/s) | $F$(N) | $T$(Nm) | $N_r$(rpm) | $U_a$(V) | $I_a$(A) | $P_{in}$(W) | $P_{out}$(W) | $\eta$ (%) | $\Delta t$ | $\Delta x$(km) |
| 5 | 0.08 | 0.89 | 0.03 | 48.52 | 0.88 | 2.39 | 4.21 | 0.32 | 7.61 | 33 $h$ 28 $min$ | 9.3 |
| 10 | 0.15 | 2.99 | 0.05 | 91.91 | 1.35 | 2.69 | 7.25 | 1.05 | 14.46 | 29 $h$ 42 $min$ | 16.5 |
| 25 | 0.39 | 15.05 | 0.18 | 216.09 | 2.81 | 4.29 | 24.1 | 8.45 | 35.06 | 18 $h$ 38 $min$ | 25.9 |
| 33 | 0.51 | 24.67 | 0.29 | 280.54 | 3.64 | 5.53 | 40.22 | 17.17 | 42.68 | 14 $h$ 28 $min$ | 26.5 |
| 50 | 0.77 | 51.85 | 0.58 | 415.24 | 5.52 | 8.97 | 99.06 | 51.34 | 51.82 | 8 $h$ 55 $min$ | 24.8 |
| 66 | 1.02 | 85.36 | 0.94 | 540.14 | 7.45 | 13.16 | 196.04 | 108.34 | 55.26 | 6 $h$ 4 $min$ | 22.3 |
| 75 | 1.16 | 107.44 | 1.18 | 609.8 | 8.59 | 15.91 | 273.43 | 153.23 | 56.04 | 5 $h$ 1 $min$ | 21.0 |
| 90 | 1.39 | 149.25 | 1.63 | 725.17 | 10.6 | 21.1 | 447.3 | 251.85 | 56.30 | 3 $h$ 47 $min$ | 19.0 |
| 100 | 1.54 | 180.52 | 1.96 | 801.64 | 12.01 | 24.96 | 599.55 | 335.97 | 56.04 | 3 $h$ 12 $min$ | 17.8 |

Table 9: Results of 9 simulations, using the complete model.

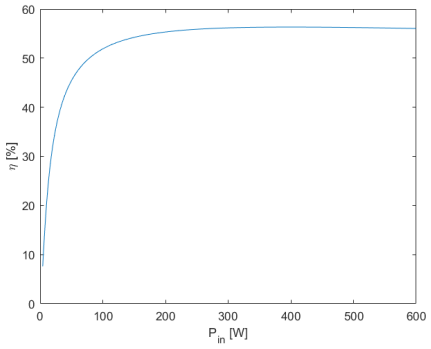


Figure 18: Efficiency of the DC motors.

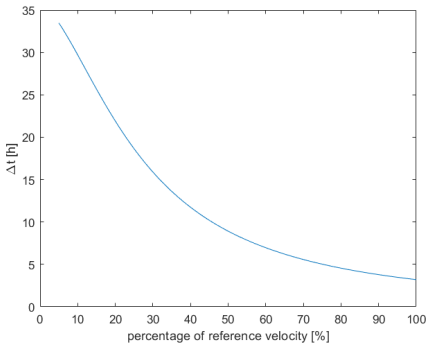


Figure 19: Endurance for different velocities.

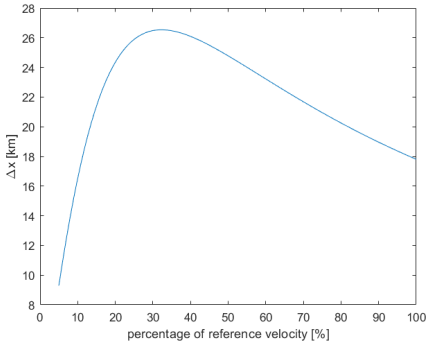


Figure 20: Distance travelled for different velocities.

It is interesting to note that the maximum distance is achieved at around 33% of the reference value, 0.51m/s (1 knot), with a value of 26.5 km. However, the system efficiency is maximum at higher speeds, namely, at around 90% of the reference value, 1.39m/s (2.7 knots), with a value of 56.30%. Furthermore, results were obtained for higher values than the reference speed. These are shown in Table 10. For these values, the efficiency now starts to decrease. Also, the armature voltage of the DC motor is higher than its rated value, which cannot be withstood by the motor for a long period, although the thrust, $F$, generated being well below the rated value of 490 N, combined. Therefore, these speeds may not be reach by this vessel.

| % of reference | Input | Output | | | | | | | | |
|---|---|---|---|---|---|---|---|---|---|---|
| | $v$(m/s) | $F$(N) | $T$(Nm) | $N_r$(rpm) | $U_a$(V) | $I_a$(A) | $P_{in}$(W) | $P_{out}$(W) | $\eta$ (%) | $\Delta t$ | $\Delta x$(km) |
| 105 | 1.62 | 197.15 | 2.14 | 839.76 | 12.73 | 27.02 | 688.01 | 384.03 | 55.82 | 2 $h$ 57 $min$ | 17.2 |
| 110 | 1.7 | 214.45 | 2.33 | 877.81 | 13.47 | 29.15 | 785.34 | 436.3 | 55.56 | 2 $h$ 44 $min$ | 16.8 |
| 120 | 1.85 | 251.01 | 2.72 | 953.71 | 14.98 | 33.66 | 1008.6 | 554.09 | 54.93 | 2 $h$ 22 $min$ | 15.8 |

Table 10: Results of 3 simulations above the reference velocity, using the complete model

## 6. Conclusions

### 6.1. Achievements

Using a theoretical and/or experimental approach it was possible to create an framework to charac-

terize the USV's main components. By the nature of each parameter it was possible to design a set of experimental tests that isolated the parameter of interest, allowing its estimation. The validity of the DC motor's estimated parameters was tested using steady state and transient state validation. Following a similar approach the hydrodynamic system was characterized. Through experimental testing and use of data gathered from prior testing it was possible to characterize the propellers. An experimental setup was developed in a water channel to gather experimental data for the propeller. The hull dynamics were characterized by theoretical analysis.

It was then added a simplified model of the batteries and the complete model was simulated for a series of velocity inputs lower than the maximum velocity achieved in experimental testing. This simulation showed that the USV's motors would have maximum efficiency for a linear velocity of around 1.39m/s (2.7 knots), the USV maximum distance travelled would be for 0.51m/s (1 knot) of 26.5km, and its maximum endurance would occur at the low end range of velocities. To test the limits of the USV it was performed a simulation for values above the maximum velocity achieved in experimental testing and the results showed that the DC motors would not be able to withstand the armature voltage needed during these conditions.

### 6.2. Future Work

One of the main difficulties found on this thesis was the lack of in water experimental data of the studied USV. It is suggested that a series of tests are executed for various velocities in an open water setup. It is also suggested the execution of tests to characterize the propeller in a wider and deeper water channel to mitigate possible perturbations, as well as tests with water flow to increase the data used to characterize the coefficient of thrust, $K_T$. Finally the use of an angular speed sensor for underwater use would allow further model validation.

## References


[1] M. Barnitsas, D. Ray, and P. Kinley. Kt, kq and efficiency curves for the wageningen b-series propellers, 1981. [Online; accessed May 23, 2022].

[2] M. Caccia, R. Bono, G. Bruzzone, G. Bruzzone, E. Spirandelli, G. Veruggio, A. Stortini, and G. Capodaglio. Sea trials of sesamo: An autonomous surface vessel for the study of the air-sea interface. *IFAC Proceedings Volumes*, 37(10):477–482, 2004. [Online; accessed May 23, 2022].

[3] M. Caccia, R. Bono, G. Bruzzone, E. Spirandelli, G. Veruggio, A. M. Stortini, and G. Capodaglio. Sampling sea surfaces with sesamo: An autonomous craft for the study of sea-air interactions. *IEEE Robotics amp; Automation Magazine*, 12(3):95–105, 2005.

[4] A. E. Fitzgerald, C. Kingsley, S. D. Umans, and B. James. *Electric machinery*, volume 5. McGraw-Hill New York, 2003.

[5] M. Kirchhoff and K. Benedict. Explaining ships dynamic and handling using matlab amp; simulink as simulation tool in teaching maritime students, 2007. [Online; accessed May 23, 2022].

[6] H. O. Kristensen and M. Lützen. Prediction of resistance and propulsion power of ships. *Clean Shipping Currents*, 1(6):1–52, 2012.

[7] H. Ma, F. Balthasar, N. Tait, X. Riera-Palou, and A. Harrison. A new comparison between the life cycle greenhouse gas emissions of battery electric vehicles and internal combustion vehicles. *Energy policy*, 44:160–173, 2012.

[8] J. E. Manley. Development of the autonomous surface craft" aces". *Oceans' 97. MTS/IEEE Conference Proceedings*, 2:827–832, 1997.

[9] J. E. Manley. Unmanned surface vehicles, 15 years of development. *OCEANS 2008*, pages 1–4, 2008.

[10] U. Nations. Resolution adopted by the general assembly on 25 september 2015. Technical report, 2015. [Online; accessed May 24, 2022].

[11] H. Ritchie, M. Roser, and P. Rosado. Energy. *Our World in Data*, 2020. [Online; accessed May 23, 2022].

[12] S. A. V. Vactor. Historical perspective on energy transitions. 2018. [Online; accessed May 23, 2022].

[13] J. C. Vasconcelos. Design of autonomous surface vessels. Extended abstract, University of Lisbon - Instituto Superior Técnico, 2015. [Online; accessed May 23, 2022].

[14] R. Yan, S. Pang, H. Sun, and Y. Pang. Development and missions of unmanned surface vehicle. *Journal of Marine Science and Application*, 9(4):451–457, 2010.